J. Synchrotron Rad. (2000). **7**, 69–77

Performance of bent-crystal monochromators for high-energy synchrotron radiation

H. Yamaoka,[a]* N. Hiraoka,[b] M. Ito,[c] M. Mizumaki,[c] Y. Sakurai,[c] Y. Kakutani,[b] A. Koizumi,[b] N. Sakai[b] and Y. Higashi[d]

[a]Harima Institute, RIKEN (The Institute of Physical and Chemical Research), 1-1-1 Kouto, Mikazuki, Sayo, Hyogo 679-5148, Japan, [b]Material Science Division, Himeji Institute of Technology (HIT), 3-2-1 Kouto, Kamigori, Ako, Hyogo 678-1297, Japan, [c]The Japan Synchrotron Radiation Research Institute (JASRI), 1-1-1 Kouto, Mikazuki, Sayo, Hyogo 679-5198, Japan, and [d]High Energy Accelerator Research Organization (KEK), 1-1 Oho, Tsukuba 305-0801, Japan. E-mail: yamaoka@spring8.or.jp

(*Received 23 August 1999; accepted 24 December 1999*)

Two monochromators for high-energy synchrotron radiation have been studied at the elliptical multipole wiggler beamline BL08W of SPring-8. Both monochromator crystals are bent and indirectly water-cooled. In the 100 keV monochromator an efficient cooling scheme is employed. A monochromatic beam is successfully focused using new benders for the 100 keV and 300 keV monochromators. Measured radii of curvature of the bent crystal agree qualitatively with calculation.

Keywords: monochromators; bent crystals; high energy; Compton scattering.

1. Introduction

In preceding papers (Yamaoka, Ohtomo & Ishikawa, 1998; Yamaoka, Mochizuki *et al.*, 1998; Sakurai *et al.*, 1995) we briefly described the design and calculations of crystal monochromators for high-energy synchrotron radiation at the wiggler beamline BL08W of SPring-8. In this paper we report the performance of these monochromators. We have two types of crystal monochromators, normally for 100 keV and for 300 keV X-rays. To focus the beam the crystals are doubly bent for the 100 keV monochromator and singly bent for the 300 keV monochromator. Both use a new type of bender. At the ESRF a similar beamline exists with specially developed bent-crystal monochromators (Suortti & Schulz, 1995; Tschentscher & Sourtti, 1996).

One of the primary concerns at third-generation rings is the heat-load problem for the optics. The heat load on the optics at BL08W is between a few hundreds watts and 1 kW even if the contribution of the lower part of the energy spectrum is reduced by filters such as graphite and Al. Heat load causes distortion of the crystal and a small deviation of the incident angle, which seriously affects the energy spread and the beam focusing, particularly for the case of a small Bragg angle in Bragg geometry. Many systems have been examined in order to reduce heat-load effects, *e.g.* using a diamond crystal, using an Si crystal with water-cooled microchannels, liquid-nitrogen cooling *etc.* (*e.g.* Yamaoka *et al.*, 1994, 1995). In the monochromators described here the crystals are indirectly water-cooled. We use Si crystals because (i) the incident angle is small, (ii) the beam footprint is large in Bragg geometry, (iii) large Si crystals are commercially available and (iv) the thermal character of Si is better than other crystal material except diamond. In the 100 keV monochromator an efficient cooling scheme is employed for the cooled channels of the crystal holder. The heat-load effect on the 300 keV monochromator is less than that on the 100 keV monochromator because of the larger beam footprint. Thus the optics were designed carefully according to the calculated results from the viewpoints mentioned above, principally heat load, beam focusing and energy spread. Experiments were performed to confirm the designed performance.

On this beamline the radiation shield is also more important because the wiggler source generates higher energy components. The monochromator crystals can be one of the scattering sources. Scattered X-rays also heat up the monochromator components. Therefore additional shield and cooling systems are used for the vacuum chambers of the monochromators.

2. Beamline

The light source is an elliptical multipole wiggler (EMPW) designed with the following parameters: period l = 12 cm, deflection parameters Kx = 0–1.1 and Ky = 11.2, number of poles N = 37, total length L = 4.5 m (Marechal *et al.*, 1995, 1998). As yet, this is the only wiggler at SPring-8. The measured magnetic field was higher than the designed value. Thus the total source power increases from the designed value of 18 kW (Kx = 1.1 and Ky = 11.2) to 24 kW (Kx = 1.234 and Ky = 13.07) for an insertion-device gap width g = 20 mm and a stored current I = 100 mA. At g =

25 mm the total power becomes the originally designed value of 18 kW and at present the wiggler is operated at this gap width. Most of the data in this paper are for $g = 30$ mm. We believe that the basic character of the optics will not change much even if the gap width changes from 30 mm down to 25 mm because the power difference is only 34%.

Figs. 1 and 2 show schematic layouts of the beamline and the optics. At the front-end there are graphite filters (total thickness 36 mm) and Al filters (total thickness 15 mm) to reduce the contribution of the low-energy components of the spectrum. There are three hutches: the white-beam (optics) hutch including the two monochromators, the monochromatic beam hutch A mainly for magnetic Compton scattering experiments, and the monochromatic beam hutch B mainly for high-resolution Compton scattering experiments.

The monochromators are single-crystal arrangements as shown in Fig. 2. The reflected beam moves when the energy is required to change and the energy ranges of the monochromators are limited geometrically. With a double-crystal arrangement it would be possible to obtain a fixed exit beam. However, the energy spread is too narrow and the number of photons is too small in the double-crystal arrangement. The beams are mostly used for inelastic (Compton) scattering experiments, where high resolution is not necessary and intensive photons are required, and the change in the energy is infrequent. The monochromators cover the energy above 100 keV as mentioned before. The relative energy spread (dE/E) and focused beam size are required to be less than 1×10^{-3} and 0.5×0.5 mm, respectively, for the 100 keV monochromator, and 5×10^{-3} and 3 mm (height) $\times$ 1 mm (width), respectively, for the 300 keV monochromator, where E is the beam energy.

Each monochromator vacuum chamber is surrounded by a 20 mm-thick lead shield; thus it is possible to decrease the lead shield thickness of the hutch. The scattered X-rays

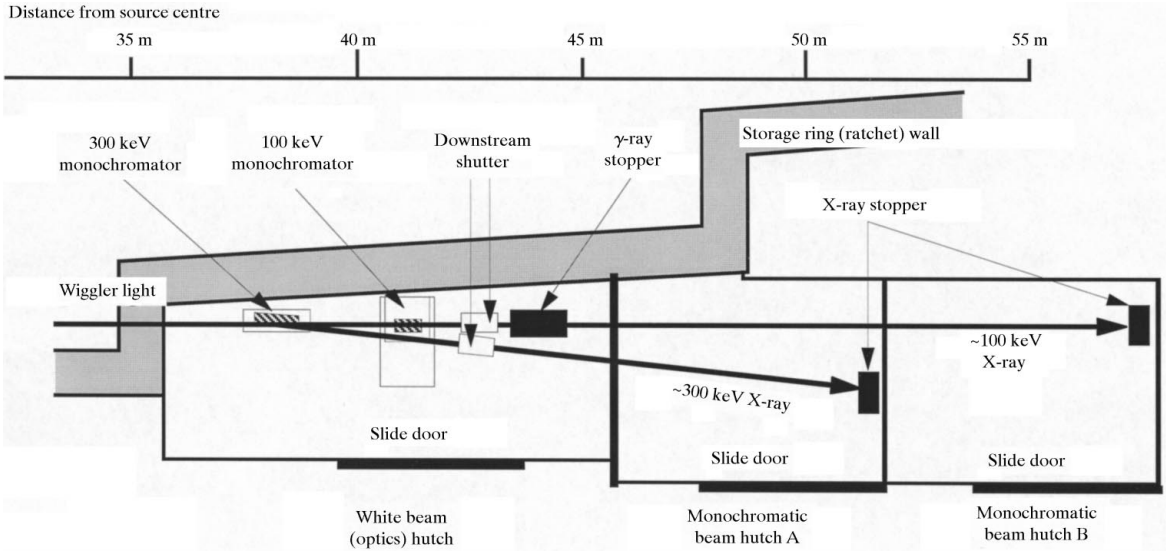

Figure 1
Schematic layout of beamline BL08W at SPring-8. Shown are the white beam (optics) hutch, monochromatic beam hutch A for the 300 keV beam and monochromatic beam hutch B for the 100 keV beam.

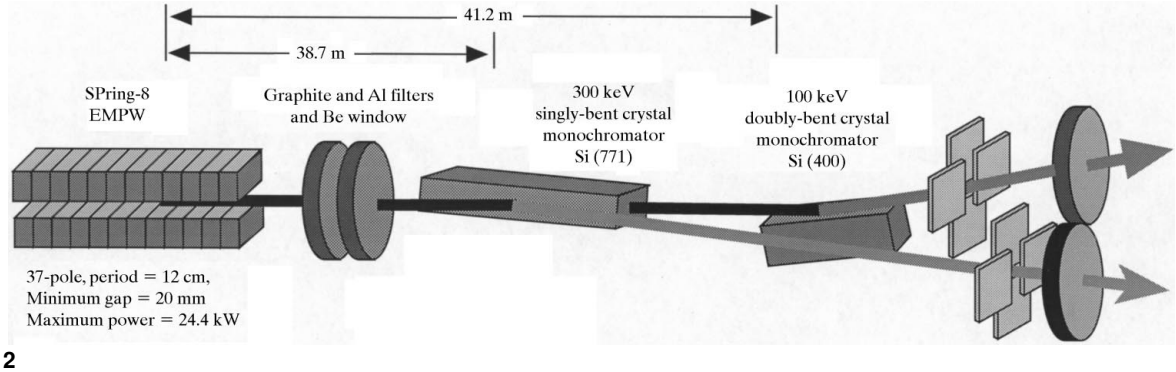

Figure 2
Conceptional view of BL08W optics with the wiggler source. Diffraction planes of the 300 keV and 100 keV monochromators are vertical and horizontal, respectively. Filters of graphite and Al are inserted before the optics to reduce the contribution of the lower-energy part of the spectrum. At present the crystal of the 300 keV monochromator has to be moved so that the white beam can pass through when the 100 keV monochromator is used.

from the crystals heat up the monochromator components and the vacuum chambers (Kawata *et al.*, 1989). Stability of the monochromators is very important because accumulating the data for Compton scattering experiments takes several hours. Thus, water-cooled Cu plates are set near to the crystal surface and the inside of the vacuum chamber wall to prevent a long-term drift of the whole system due to heating.

3. Optics

3.1. *100 keV monochromator*

The monochromator consists of a shielded vacuum chamber containing the Si crystal, the crystal holder, the primary copper shield, the bender, the translation stage, in-plane rotation and up/down stages, and the water-cooled copper skin attached to the vacuum chamber wall. The monochromator chambers are evacuated to $\sim 10^{-3}$ Pa to reduce the background due to Compton scattering by air. All mechanisms are mounted onto a side flange bolted to the rotation mechanism (Bragg angle). Access to the mechanisms is *via* the side flange through which Bragg rotation is introduced. A ferrofluidic vacuum seal is used on the Bragg rotation shaft. The Bragg angle can be varied from -3° to 7° with a resolution of 0.04 arcsec per step. The side flange can be manually withdrawn horizontally along a rail system.

Bragg geometry is employed for the monochromators because the crystal cannot easily be doubly bent to obtain efficiently a focused beam in the Laue case. The 100 keV monochromator crystal is set horizontally and the reflected beam moves vertically. The scanning energy range is from $\sim$100 keV to 120 keV, being limited geometrically for the Si(400) reflection. The monochromator is a symmetric Johann type and doubly bent. A thin 3 mm-thick Si crystal with grooves is mounted onto a water-cooled crystal holder that has a fixed sagittal radius. The Si[100] crystal plane is used as a diffraction plane. The holder with the crystal is bent meridionally by the bender.

We follow the method developed at KEK AR NE1 beamline (Kawata *et al.*, 1998). Here, however, we have made some improvements: the cooled channels of the holder were changed from holes to small slots to obtain a higher heat-transfer coefficient, and a new crystal bender was introduced. The crystal size is 100 mm in width and 225 mm in length. The crystal is grooved; the surface grooves are 0.6 mm in width, 2.7 mm in depth and 1.8 mm in pitch along the beam direction; the back grooves are 0.5 mm in width, 0.5 mm in depth and 5.5 mm in pitch along the sagittal direction. There are overlaps of 0.2 mm between the surface and back grooves at the cross points. Liquid In-Ga is used between the crystal and the crystal holder, Ni-coated to improve thermal contact and to ensure that the crystal sticks well into the holder shape by surface tension. The crystal is mounted by clamping both sides. Once it is set on the holder through In-Ga it is difficult to take off without breaking.

The formula for the sagittal bending radius to minimize the energy spread is written as

$$N = (1 - \cos\theta_B)\, p / \sin\theta_B, \qquad (1)$$

where N, θ_B and p are the sagittal radius, the Bragg angle and the distance from the source to the crystal, respectively (Yamaoka, Ohtomo & Ishikawa, 1998). The analyses showed that the minimum energy spread is obtained when the sagittal focus is $q/p \simeq 1/3$, where q is the distance from the crystal to the focused point. Sparks *et al.* (1980) reported the same result but with a different method. The crystal holder has a fixed radius of $\sim$820 mm in the sagittal direction calculated using (1) under the conditions of p = 41.2 m, E = 115.5 keV and with an Si(400) reflection. Even if the reflection energy is changed in a range from 100 to 150 keV, the energy spread is kept to be within the required value of 10^{-3} when the crystal is ideally fit to the holder shape. For meridional focus, q/p = 1 corresponds to the minimum energy spread. If we use an asymmetric reflection, the meridional focus point will coincide with the sagittal one. We do not use an asymmetrically cut crystal because a smaller beam is not necessary in the first phase experiments.

The crystal holder has 33 slot channels for water cooling, each being 1 mm in width, 5 mm in height and 3 mm in pitch. The minimum thickness between the surface and the channel is $\sim$1.2 mm. The channel length along the beam direction is $\sim$300 mm. It is difficult to cut such long slot channels directly into the Cu block. Therefore a two-step procedure has been taken here. First, slot channels were grooved onto a Cu block surface and then a flat Cu block was welded by silver solder to close the channels. No accidents such as water leakage into the holder have occurred for more than a year. The total flow rate is 12 l min^{-1}. The fluid velocity is 1.2 m s^{-1}, this value being small enough to prevent corrosion by the water flow. To achieve an ideal curvature the crystal holder surface was polished like a mirror surface at the KEK Mechanical Engineering Center.

Fig. 3 shows a schematic layout of a newly developed crystal bender with the crystal holder for the 100 keV monochromator. The radius of the crystal curvature and the beam footprint become larger as the reflection energy is

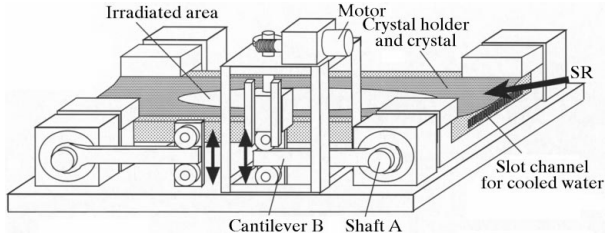

Figure 3
Schematic view of the crystal bender for the 100 keV monochromator. The thin 3 mm-thick crystal is clamped from both sides. Each lever of the bender can be controlled independently. SR = synchrotron radiation.

higher. Thus more precise control over a large area is required to achieve an ideal crystal curvature. The bender design is based on a four-point bending mechanism. Either end of the crystal holder is operated independently by two stepping motors each in a sine-bar configuration to correct the asymmetry of the bent crystal. The bender is designed to have a radius of curvature from 500 m to 1000 m meridionally. A small linear up/down motion of cantilever B produces a rotation or a twist of shaft A and the crystal is bent with the crystal holder. A small angle deviation produces a large energy shift because the incident angle is very small in the monochromator to reflect high energy. In this bender the temperature change in shaft A has little effect on the crystal holder position, *i.e.* on the incident angle. This function is important particularly for the monochromator with a small incident angle. The performance of the bender was first confirmed in an off-line experiment. The moment, the force of cantilever B (12 cm in length) to bend the crystal with the holder, and the twist of shaft A are estimated to be ∼80 N m, 670 N and 0.45 mrad, respectively. A 1/50 worm gear is placed between the motor and the up/down bar to move cantilever B. The long cantilever B allows the use of a small worm gear. The base plate of the bender is designed in such a way that the bender force does not cause any displacement of the plate.

3.2. *300 keV monochromator*

The 300 keV monochromator is an asymmetric Johann-type monochromator. The crystal surface is vertical and the reflected beam moves horizontally. The scanning energy range is from ∼270 keV to 300 keV. The crystal is protected from the background radiation by a water-cooled copper tube, with a rectangular cross section to act as a primary shield. The Bragg rotation, the crystal up/down actuation and the horizontal translation are all performed within the vacuum chamber. The Bragg rotation is performed by a stepping motor in a sine-bar configuration and capable of rotating from -1° to 6° with a resolution of 0.36 arcsec per step. All mechanisms are on a thick base plate which provides an up/down motion *via* three supports. The up/down actuator is initiated outside the vacuum. The three supports are coupled with the base plate through bellows forming a kinematic mount. All motions are therefore decoupled from the vacuum chamber. The crystal is large, 800 mm in length, 60 mm in width and 30 mm in height, cut from a 5 inch Czochralski Si ingot grown in the [001] orientation. The Si(771) reflection is used with an asymmetry angle of $\sim 1^\circ$. The relation for asymmetrically cut crystal focusing is written as

$$\sin(\theta_B + \alpha)/p + \sin(\theta_B - \alpha)/q = 2/R, \qquad (2)$$

where α and R are the asymmetry angle and the radius of curvature of the diffracting plane, respectively (Matsushita & Hashizume, 1983). The asymmetry angle brings the focused point upstream, and makes the incident angle of the crystal larger and the crystal length shorter. The radius is estimated to be 664 m under the conditions of $\theta_B = 2.17^\circ$, $p = 38.7$ m, $q = 12.9$ m and $\alpha = 1^\circ$.

Fig. 4 shows a schematic layout of the crystal bender with the crystal holder on the translation and Bragg rotation stages. Essentially the crystal holder and bending mechanism for the 300 keV monochromator are similar to those for the 100 keV monochromator except for shaft A and the lever B which are vertical and horizontal, respectively, in the 300 keV monochromator. In the beamline the space between the 300 keV monochromator and the ratchet shielding wall is very small. The bender also resolves this problem because we can make the space small. The moment and force of cantilever B (24 cm in length) to bend the crystal with the holder are estimated to be ∼180 N m and 740 N, respectively. A 1/50 worm gear is placed between the motor and bar A to move cantilever B.

3.3. *Crystal curvature and crystal holder*

The calculated results showed that the ideal curvature is obtained at the centre with a width of about ±50 mm for the 100 keV monochromator and ±200 mm for the 300 keV monochromator under the heat load (Yamaoka, Mochizuki *et al.*, 1998). If there is heat load, an additional bending force is necessary to compensate for the heat-load effect.

Normally the curvature at both ends of the crystal bender (including clamping points) is far from ideal when the crystal is bent. The crystal or the crystal holder length should be much longer than the beam footprint. The length of the beam footprint is ∼50 mm at 115.4 keV for the 100 keV monochromator and ∼420 mm at 274 keV for the 300 keV monochromator. They are smaller than the distances of ∼310 mm and 700 mm between the clamped points for the 100 keV monochromator and the 300 keV monochromator, respectively. The effect from the clamped

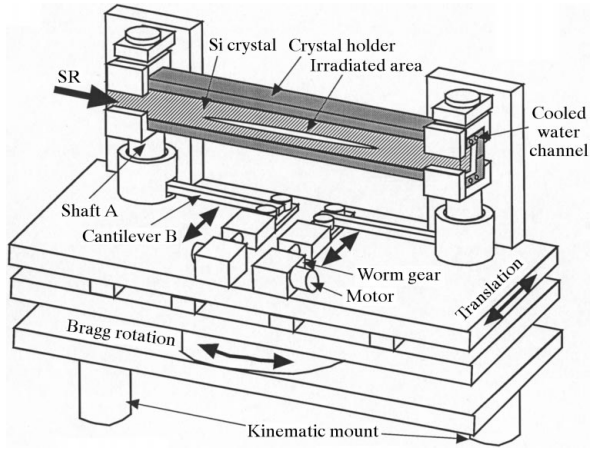

Figure 4
Schematic view of the crystal bender for the 300 keV monochromator. The thick Si crystal is clamped on the water-cooled crystal holder; it is on the translation and Bragg rotation stages. All motions are decoupled from the vacuum vessel *via* a kinematic mount. SR = synchrotron radiation.

parts is small as will be shown in the following section. The crystal holder normally has a curvature before setting a crystal even if a bending force is not applied. The bender should be designed so as to compensate this original curvature, otherwise the holder should be finished as flat as possible. Our crystal holders also have curvatures and the benders can correct them to within mechanical allowance.

4. Results and discussion

4.1. *Calorimetry*

The incident power on the crystal was measured using thermally isolated calorimetry. A Cu block was placed in the white beam. Based on the temperature increase with time, the real power that the Cu block absorbs was calculated by using the code *OEHL* (Tong *et al.*, 1992, 1995). Additional corrections were needed for the Compton back-scattered power, Compton transmitted power, Rayleigh back-scattered power and Rayleigh transmitted power, 1.54%, 0.08%, 0.05% and 0.03% of the incident power, respectively. The result shows that most power is used to heat up the Cu block. The measured powers were 350 W in linear polarization mode and 160 W in circular polarization mode under the conditions of I = 70 mA, g = 30 mm and with the front-end vertical slit of 1.5 mm at p = 30.6 m. Calculations show that there are differences of several tens of percent between the measured values and calculations. The measured values are lower than the calculations. This may be due to the offset of the front-end slit from the beam centre in these measurements and the values of the filter material densities at the front-end used in the calculation.

4.2. *100 keV monochromator*

The reflected beam from the 100 keV monochromator has two components. One is from the surface (upper part). The other, from the bottom of the grooves (lower part), degrades the energy resolution because the reflection is optimized for the surface. The lower part of the reflection should be cut by a slit system to obtain a better energy resolution, as required. The energy spread is derived from the measurement of the UO_2 K-absorption edge by using free air ion chambers. The linearity of the ion chambers for the incident beam intensity is checked by comparing three detectors: the ion chambers, an SSD (solid-state detector) (Ge) and a photodiode. The linear relation among them is confirmed in intensity range over three orders of magnitude. When the energy is changed, the reflected beam moves vertically. The movement of the measurement system, the slit and the ion chambers, is synchronized with that of the Bragg angle of the monochromator crystal.

The UO_2 sample contains ^{238}U (99.3%) and ^{235}U (0.7%). The major contribution to the energy spread comes from ^{238}U. The natural width is calculated to be 96.1 eV for the K-level (Krause & Oliver, 1979). We also measured the K-absorption edge of UO_2 using the third harmonics of Si(311) diffraction of a double-crystal monochromator at the EXAFS beamline BL01B1 of SPring-8. The rocking-curve width of Si(331) diffraction is 0.83 arcsec. The measured value is 84 eV. We cannot explain the difference of ~10% between theory and measurement at present. The energy spread of the monochromator is estimated by deconvoluting the differential curve of the K-edge absorption. Typical results are shown in Fig. 5. The measured energy spread, dE/E, is 1.4×10^{-3} at g = 30 mm when the lower part of the reflection is cut. An energy spread smaller than 10^{-3} is required for high-resolution Compton scattering experiments. An energy spread $dE/E \simeq 1 \times 10^{-3}$ is achieved when the beam is cut horizontally and the photon flux is about half of that before it is cut. The results indicate that there is still deformation of the crystal. This is due to the fact that the crystal does not fit well to the holder shape and that there is a heat-load effect although an efficient cooling scheme is employed for the crystal holder.

Simulation by using the Takagi–Taupin equation shows that a change in the radius of curvature of less than a few tens of metres affects the energy spread (Yamaoka, Ohtomo & Ishikawa, 1998). The wide energy spread is therefore due to the deformation occurring when the crystal is mounted and/or bent. Note that the crystal mounting condition on the holder changes gradually as a function of time. Just after the crystal was first mounted onto the holder, the crystal did not fit to the holder shape and we could not find an optimum condition although many parameters were surveyed. The fit, however, becomes better with time.

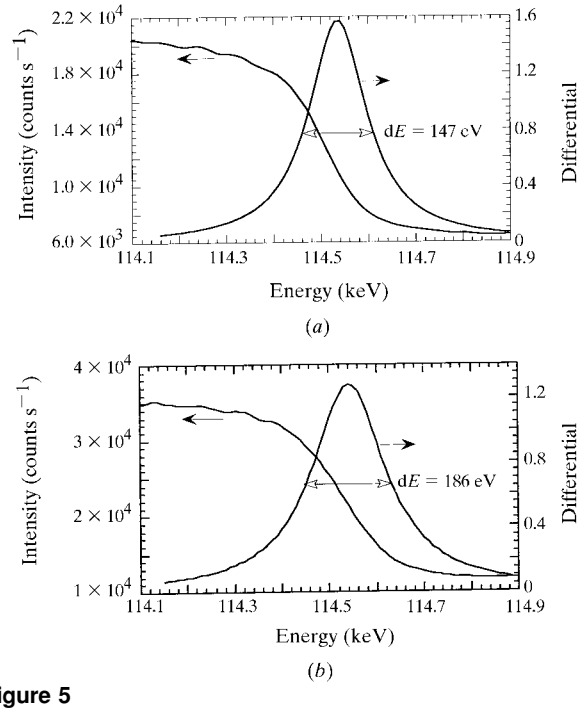

Figure 5
Examples of UO_2 K-edge absorption curves with differential curves. The horizontal slit size is (*a*) half and (*b*) fully opened under the conditions of a bender pulse of 700 and I = 65 mA. The energy spreads (dE/E) are estimated to be 0.97×10^{-3} for (*a*) and 1.4×10^{-3} for (*b*).

The photon flux of the reflected beam was directly measured by the SSD placed behind a 550 mm-thick Al absorber. The photon flux is evaluated to be $\sim 8 \times 10^{12}$ photons s^{-1} at 115.7 keV under the conditions of linear polarization, g = 30 mm and I = 70 mA, assuming an Al absorption coefficient of 0.4366 cm^{-1} and SSD detection efficiency of 80%. The photon flux was also measured indirectly by the Compton scattering from an Al target. It shows that the photon flux is $\sim 8.2 \times 10^{12}$ photons s^{-1} at 115.5 keV for an insertion-device gap g = 25 mm and an energy spread of 1.5×10^{-3}. This value corresponds to a flux of $\sim 4.8 \times 10^{12}$ photons s^{-1} for g = 30 mm and I = 70 mA. The total flux should be $\sim 7.2 \times 10^{12}$ photons s^{-1} if there are no grooves on the crystal.

We can estimate the energy spread and photon flux by using analytical formulae for a bent crystal (Erola *et al.*, 1990). They are calculated to be $dE/E \simeq 4 \times 10^{-4}$ and 6×10^{12} photons s^{-1}, respectively, for a bending radius of 500 m. The energy spread is different because the fit of the crystal to the holder is not perfect in practice. The measured value of the flux is smaller than the estimation when we consider the energy spread. This may be explained by considering the uncertainties or errors of the parameters used in the estimation such as filter densities, front-end slit size, bending radius (the crystal is two-dimensionally bent) *etc*.

The crystal length and the beam footprint are 225 mm and ~50 mm, respectively. The crystal did not fit well to the holder shape. An optimum position along the beam direction to minimize the energy spread was found by changing the beam position on the crystal. The energy spread was estimated using the measurements of the UO_2 K-absorption edge as a function of the crystal surface position and the bender pulse as shown in Fig. 6. It is better upstream (negative x, where x is a crystal surface position in the meridional direction) of the crystal than downstream. Heat-load effects were observed for different stored currents at x = 0 mm. This effect, however, was found to be small at a stepping-motor pulse of ~500 of the bender where the energy spread became minimum. A stepping-motor pulse corresponds to a bender up/down motion of ~7 nm per step at the crystal centre.

It is interesting to measure the radii of curvatures of the bent crystal so that the actual crystal condition on the beamline is known. We measured the energy shift of the reflected beam by the SSD as a function of the crystal surface position with a very narrow incident beam for a given bender pulse. The energy shift (dE) corresponds to the angle deviation $\delta\theta$. The surface displacement δy is derived from $\delta\theta$ [see equation (3)] and in this way the radius of curvature is estimated according to equation (4),

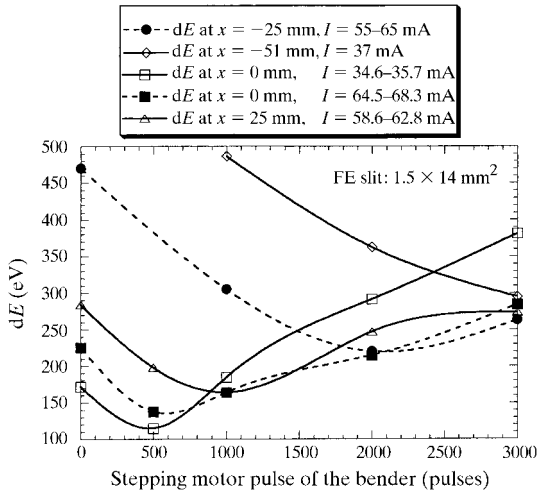

Figure 6
The energy spread as a function of the bender pulse and the position on the crystal surface. We can observe the heat-load effect at x = 0 mm for two kinds of stored currents although the difference is small at the stepping-motor pulse of 500 of the bender. FE = front-end.

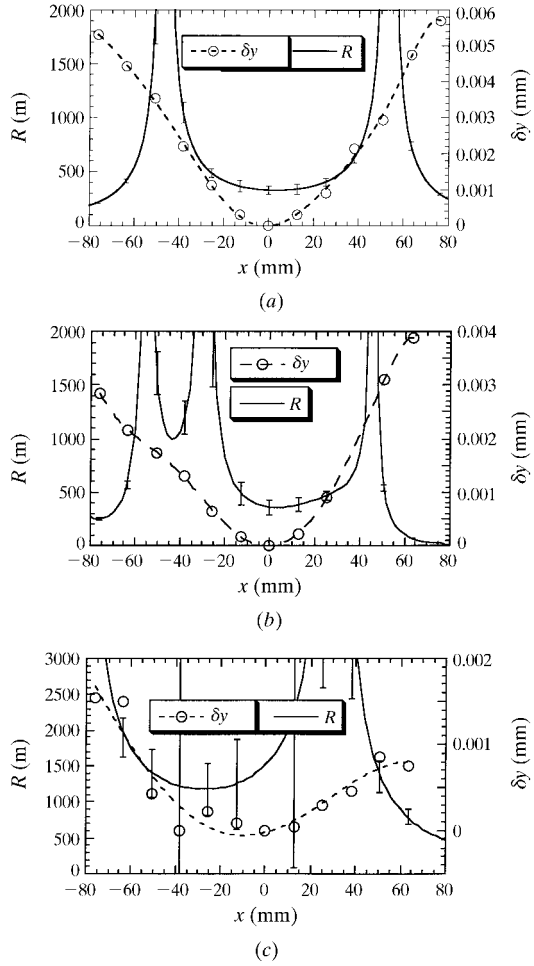

Figure 7
The displacement δy and the radius of curvature R as a function of crystal surface position for stepping-motor pulses of (*a*) 3000, (*b*) 2000 and (*c*) 500 of the bender. The displacements are estimated from the measurements of the energy shift with a narrow slit. Open circles are measured points and the dashed line for δy is a fit curve. The solid line is a fit curve for R. The beam footprint is ~50 mm on the crystal.

where y is a coordinate vertical to the beam direction. The relations are written as follows,

$$\delta y = R(1 - \cos\delta\theta) \simeq R(\delta\theta)^2/2. \quad (3)$$

Here, $dE/E = \cot\theta_B \delta\theta$ and $x = R\delta\theta$, where x is a coordinate parallel to the beam direction on the crystal surface. Therefore we have the relation

$$\delta y = (x/2)\tan\theta_B(dE/E),$$
$$R = [1 + (\delta y)''^2]^{3/2}/(\delta y)'' \simeq 1/(\delta y)''. \quad (4)$$

Fig. 7 shows the results for stepping-motor pulses of 500, 2000 and 3000 of the bender. Note that the reliability of the measurement becomes poor as the radius moves to an ideal one shown at the stepping-motor pulse of 500 in Fig. 7(*c*) because the energy shift also becomes smaller and it is difficult to measure the shift precisely due to the SSD energy resolution. The results qualitatively reproduce that of the finite-elements analyses (Yamaoka, Mochizuki *et al.*, 1998).

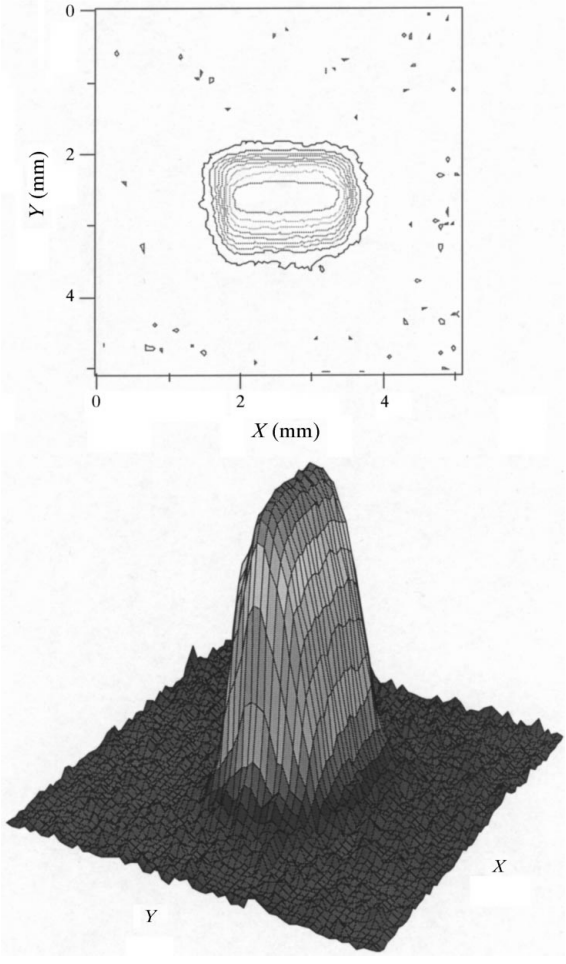

Figure 8
An example of the focused beam profiles at 115.5 keV (q = 16.1 m) with a contour map measured by X-ray film. The coordinates of X and Y correspond to horizontal and vertical directions, respectively.

An example of focused beam profiles is shown in Fig. 8. The photographs are taken using Fuji industrial X-ray films behind a 3 mm-thick Pb absorber with typical exposure times of ~10 s. The typical beam size is ~1.7 mm horizontally and 1.0 mm vertically at the focused point. Note that the crystal is grooved with a surface width of 1.2 mm and a groove width of 0.6 mm (1.8 mm pitch) along the beam direction. Therefore the horizontally focused beam width of ~1.7 mm is close to the minimum value.

4.3. *300 keV monochromator*

The diffracted beam from the 300 keV monochromator passes through the 100 keV monochromator vacuum chamber because of geometrical restriction. The photon flux is directly measured after penetrating a 22 mm-thick Pb absorber by an SSD. It is estimated to be ~4.5 × 10^9 photons s^{-1} at 274 keV under the conditions of linear polarization, g = 30 mm and I = 70 mA, assuming a Pb absorption coefficient of 5.81 cm^{-1} and an SSD detection efficiency of 14%. Estimation of the photon flux with an analytical formula (Erola *et al.*, 1990) gives ~4 × 10^{10} photons s^{-1} for a bending radius of 720 m. This value is much higher than the measured one; we do not understand fully this difference at present even if there are some ambiguities in the parameters in the estimation. Further study will be necessary.

Surface polishing by using polishing paper (♯600, mean abrasive particle size of ~40 μm) was used in an attempt to obtain a higher flux. No effect, however, was observed. The diffraction occurs at a depth much greater than several tens of micrometres.

The radii of curvature for the 300 keV monochromator were measured by the same method as those in the 100 keV monochromator. Fig. 9 shows an example of the displacement and the radius of curvature as a function of the crystal surface position. The displacement is fitted well by a parabolic curve and the radius takes a constant value of ~720 m, which is in good agreement with the calculated value of 664 m [equation (2)]. The crystal of the 300 keV monochromator is singly bent, and the beam footprint is

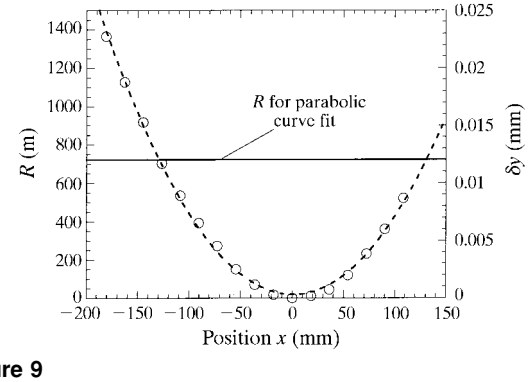

Figure 9
The displacement δy and the radius of curvature R as a function of crystal surface position for the 300 keV monochromator. Open circles are measured points and the dashed line for δy is a curve fit by a parabola, which gives a constant R of 721 m (solid line).

Table 1
Summary of the results of dE/E, photon flux and focused beam size at beamline BL08W, SPring-8, with those at AR NE-1, KEK (Kawata *et al.*, 1998).

The data at SPring-8 are taken under the following conditions: stored current I = 70 mA and insertion-device gap width g = 30 mm.

	Energy (keV)	Crystal	dE/E (10^{-3})	Photon flux (photons s^{-1})	Focused beam size (V × H) (mm)
KEK AR NW1	60	Si(111)	1	5×10^{12}	0.5 × 2
SPring-8 BL08W	115	Si(400)	1	2×10^{12}–4×10^{12}	1.0 × 1.7
	274	Si(771)	2	5×10^{9}	2.3 × 1.5

~400 mm which is much shorter than the distance between the clamped points. Therefore the curvature of the bent crystal becomes almost ideal near the crystal centre.

An example of a focused beam profile is shown in Fig. 10. The typical exposure time of Fuji industrial X-ray film behind a 2 mm-thick Pb absorber is several seconds. The focused beam size is ~1.5 mm in width and 2.3 mm in height. The asymmetrical profile in the x direction may be due to absorption effects and the asymmetry of the crystal. The energy spread of the elastic peak is measured by an SSD, and $\delta E/E$ is evaluated to be $\sim 2 \times 10^{-3}$. This value is much better than the required value of 5×10^{-3} for magnetic Compton scattering experiments. At present the 300 keV monochromator has to be moved horizontally when the 100 keV monochromator is used. The reproducibility is, however, good when the 300 keV monochromator is back in its original position.

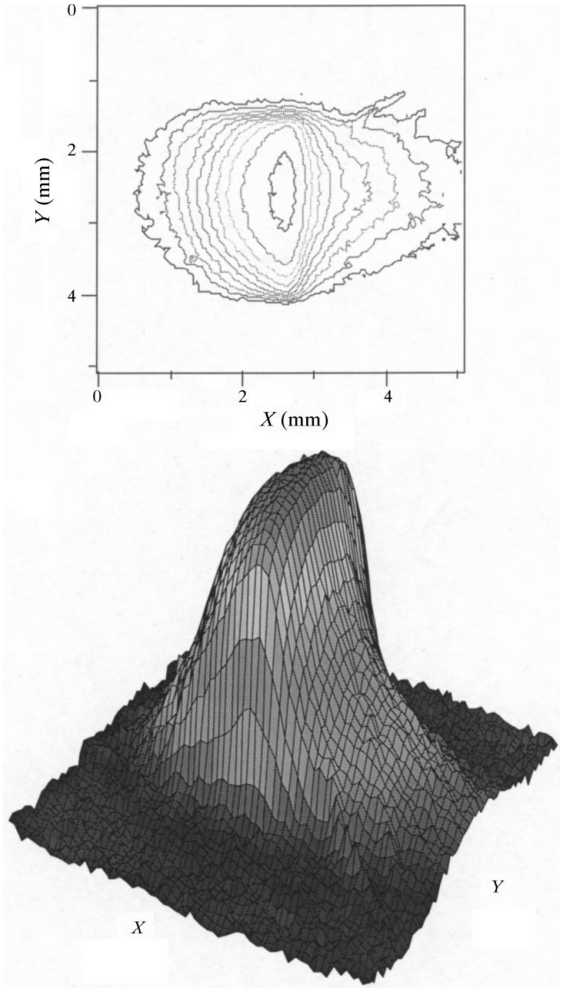

Figure 10
An example of the focused beam profiles at 274 keV with a contour map measured by X-ray film.

The degree of circular polarization, Pc, was measured at 274 keV by the method of spin-dependent Compton scattering applied to a polycrystalline Fe sample. The evaluated maximum Pc is 0.8 at the beam centre, where we use an Fe magnetic moment of $1.8\mu_B$ at room temperature, where μ_B is the Bohr magnetron. The measured Pc agrees well with the calculated value for a 2% coupling constant of the electron beam in the storage ring (Mizumaki *et al.*, 1998). (Now the coupling constant is much better.)

5. Summary

We have studied monochromators operating at around 100 keV and 300 keV for high-energy synchrotron radiation at SPring-8. The reflected beams are successfully focused by the benders developed here. The radii of curvature of the bent crystals were measured on the beamline. They agree qualitatively with the calculations. The benders perform best at the crystal centre. There is still deformation of the crystal in the 100 keV monochromator and this causes a wider energy spread. Further development will be necessary for the crystal fit to the holder and for an effective cooling scheme.

In Table 1, results from SPring-8 BL08W are compared with those from KEK AR NE1 concerning dE/E, photon flux and the focused beam size. The focused beam size at SPring-8 is comparable with that at AR NE1 although the reflection energy at SPring-8 is much higher. The performance of both kinds of monochromators almost satisfies the requirements for the present Compton scattering experiments. The photon flux at 274 keV is, however, relatively small because we utilize higher indices of the Si crystal. A possible method of increasing the 300 keV photon flux is to use an annealed Si crystal (Yamaoka *et al.*, 1997).

Higher reflection energies at SPring-8 provide opportunities to study 4d, 4f and heavy elements of the metals by Compton scattering (Sakurai, 1998). These high energies have been used not only for Compton scattering experi-

ments but also for nuclear physics, analysis by using X-ray fluorescence, diffraction in non-crystalline materials *etc.* These experiments indicate that background is a serious problem. Careful design to reduce the background will be necessary in the experimental apparatus.

The authors are grateful to Dr T. Ishikawa of RIKEN for useful suggestions about the monochromator design. We thank Professor H. Kawata and Mr M. Sato of the Photon Factory at KEK for their help with the off-line characterization experiment for the 100 keV monochromator. The measurement of the *K*-edge of UO_2 was performed under collaboration with Dr T. Uruga and Dr H. Tanita of JASRI and we thank them for their kindness. We also acknowledge Mr H. Shibaoka of Fuji Film for his offer of industrial X-ray film and Mr M. Seigo of HIT for his assistance with the experiment.

References

Erola, E., Eteläniemi, V., Sourtti, P., Pattison, P. & Thomlinson, W. (1990). *J. Appl. Cryst.* **23**, 35–42.

Kawata, H., Miyahara, T., Yamamoto, S., Shioya, T., Kitamura, H., Sato, S., Asaoka, S., Kanaya, N., Iida, A., Mikuni, A., Sato, M., Iwazumi, T., Kitajima, Y. & Ando, M. (1989). *Rev. Sci. Instrum.* **60**, 1885–1888.

Kawata, H., Sato, M., Higashi, Y. & Yamaoka, H. (1998). *J. Synchrotron Rad.* **5**, 673–675.

Krause, M. & Oliver, J. H. (1979). *J. Phys. Chem. Ref. Data*, **8**, 329–338.

Marechal, X. M., Hara, T., Tanabe, T., Tanaka, T. & Kitamura, H. (1998). *J. Synchrotron Rad.* **5**, 431–433.

Marechal, X. M., Tanaka, T. & Kitamura, H. (1995). *Rev. Sci. Instrum.* **66**, 1937–1939.

Matsushita, T. & Hashizume, H. (1983). *Handbook on Synchrotron Radiation*, Vol. 1, edited by E. E. Koch, pp. 261–314. Amsterdam: North-Holland.

Mizumaki, M., Yamaoka, H., Sakurai, Y., Ohata, T., Koizumi, A., Hiraoka, N., Kakutani, Y., Seigo, M. & Sakai, N. (1998). *SPring-8 Annual Report 1997*, p. 293. JASRI, Mikazuki, Sayo, Hyogo 679-5198, Japan.

Sakurai, Y. (1998). *J. Synchrotron Rad.* **5**, 208–214.

Sakurai, Y., Yamaoka, H., Kimura, H., Marechal, X. M., Ohtomo, K., Mochizuki, T., Ishikawa, T., Kitamura, H., Kashiwara, Y., Harami, T., Tanaka, Y., Kawata, H., Shiotani, N. & Sakai, N. (1995). *Rev. Sci. Instrum.* **66**, 1774–1776.

Sparks, C. J., Borie, B. S. & Hasting, J. B. (1980). *Nucl. Instrum. Methods*, **172**, 237–242.

Suortti, P. & Schulze, C. (1994). *J. Synchrotron Rad.* **2**, 6–12.

Tong, X. M., Yamaoka, H., Nagasawa, H. & Watanabe, T. (1995). *J. Appl. Phys.* **78**, 2288–2297.

Tong, X. M., Yamaoka, H. & Sakurai, Y. (1992). *Proc. Soc. Photo-Opt. Instrum. Eng.* **1739**, 514–521.

Tschentscher, Th. & Sourtti, P. (1996). *Rev. Sci. Instrum.* **67**, 21–29.

Yamaoka, H., Freund, A. K., Holmberg, J., Rossat, M., Wulff, M., Hanfland, M., Lee, W.-K. & Mills, D. M. (1995). *Nucl. Instrum. Methods*, A**364**, 581–584.

Yamaoka, H., Goto, S., Kohmura, Y., Uruga, T. & Ito, M. (1997). *Jpn. J. Appl. Phys.* **36**, 2792–2799.

Yamaoka, H., Häusermann, D., Freund, A. K., Kremrey, M. & Kvick, Å. (1994). *Nucl. Instrum. Methods*, A**351**, 559–564.

Yamaoka, H., Mochizuki, T., Sakurai, Y. & Kawata, H. (1998). *J. Synchrotron Rad.* **5**, 699–701.

Yamaoka, H., Ohtomo, K. & Ishikawa, T. (1998). *J. Synchrotron Rad.* **5**, 687–689.